SCIENTIFIC REPORTS

OPEN

SUBJECT AREAS:
NANOPARTICLES
OPTICAL PHYSICS
NANOPHOTONICS AND PLASMONICS

Received
21 October 2014

Accepted
13 January 2015

Published
3 February 2015

Correspondence and requests for materials should be addressed to Z.L. (zpli@cnu.edu.cn) or H.Z. (hzhang@szu.edu.cn)

Giant local circular dichroism within an asymmetric plasmonic nanoparticle trimer

Hancong Wang[1,2], Zhipeng Li[1,2], Han Zhang[1,3], Peijie Wang[2] & Shuangchun Wen[1]

[1]Key Lab of Micro-/Nano- Optoelectronic Devices of Ministry of Education, School of Physics and Electronics, Hunan University, Changsha 410082, China, [2]The Beijing Key Laboratory for Nano-Photonics and Nano-Structure (NPNS), Center for Condensed Matter Physics, Department of Physics, Capital Normal University, Beijing 100048, China, [3]SZU-NUS Collaborative Innovation Center for Optoelectronic Science & Technology, Key Laboratory of Optoelectronic Devices and Systems of Ministry of Education and Guangdong Province, College of Optoelectronic Engineering, Shenzhen University, Shenzhen 518060, China.

We investigated the near-field response in silver nanoparticle aggregates to the excitation of circular polarized light. In a right-angle trimer system, the local field intensity excited by right-hand circularly polarized light is almost one thousand times larger than the left-hand case. By analyzing the polarization and phase of the local field in plasmonic hotspots, we found this local circular dichroism is originated from the near-field interference excited by orthogonal polarized incident lights. The local circular dichroism can be tuned by the rotation of the third particle, the interparticle distance, and the dielectric environment. This phenomenon could also widely exist in more complicated nanoaggregates. These findings would benefit for resolving light handedness, and enhancing circular dichroism and optical activity.

Chiroptical effects are typically characterized by small differences of extinction coefficients or refractive indexes in the interaction of left-hand circularly polarized light (LCP) and right-hand circularly polarized light (RCP) with chiral molecules, leading to circular dichroism (CD) or optical activity (OA)[1]. The CD spectroscopy is widely used to investigate the subtle structural information of organic and biological molecules[2]. High concentration and large quantity of chiral specimens are usually demanded for reliable signal-to-noise. Concepts borrowed from molecular science, giant CD or OA response have been observed in metallic nanostructures such as spirals[3], crosses[4–6], nanorods[7], helixs[8,9], oligomers[10,11], pyramidals[12], *etc*[13]. The mechanism of either exciton-plasmon interaction between chiral molecules and metal nanostructures[14,15], or near-field interactions in plasmonic nanostructures with chiral geometry[16–18], makes the CD or OA response much stronger than the one from merely chiral molecules. The surface enhanced Raman optical activity (SEROA) of chiral molecule is contributed to the plasmonic hotspots in metal nanoparticles[19,20]. The change of symmetry in nanoaggregates would alter the polarization response of Raman scattered light[21]. Also, new chiral center might generate for different sorption sites in aggregates, which makes it challenging to obtain the stability and repeatability of SEROA. Recently, it was found even for an achiral molecule in a planar nanoparticle trimer, Raman scattering of the molecule can carry a considerable degree of circular polarization, that is, scattered circular polarization Raman optical activity (SCP ROA)[22,23]. The origin of this plasmonic ROA in the molecule-aggregates system is also the nanoantenna effect of asymmetric particles excited by the Raman emission of the molecule[24]. The single-molecule ROA may open a new perspective on the characterization for structural biology and pharmaceutical industry[25]. Actually, local field in the nanogap of aggregates could also have CD characteristic, which might result in incident circular polarization ROA[26,27] and local scattering OA[28]. For example, the large scattering OA has been locally observed in random fractal aggregates of silver nanoparticles by photon scanning tunneling microscopy. OA properties of aggregates have been simulated to reproduce the experiment observations[28–31]. However, in the complicated coupled nanoparticles system[32–35], a fundamental insight into the relation between the near field and geometry under the excitation of circularly polarized light (CPL), is still needed for deeply understanding the origination of these OA phenomena, which will also be beneficial for the design of plasmonic CD or ROA nanostructures.

In this paper, the local field response to the CPL excitation in nanoparticle dimer and trimer was investigated. We found the near-field enhancement in an asymmetric trimer is highly dependent on the polarization rotation. The local field at a hotspot excited by RCP is much larger than the LCP case. The dependence originates from the near-field interference in the strong coupled nanoantenna system and can be tuned by the rotation of the third

particle, the interparticle distance, and the dielectric environment. Similar to far-field CD, we introduce a parameter ρ in order to evaluate the local CD. Both positive and negative ρ are found in the asymmetric nanoantenna system. Besides, ρ is very sensitive to the environment. This study could provide a more flexible way to design plasmonic nanostructures with strong CD or ROA response for various applications such as polarization sensitive devices[3,8] and plasmonic sensors[36,37].

Results

To understand the near-field response of nanoparticle aggregates to the CPL, analytic electromagnetic solutions to multi-sphere system simulations based on the generalized Mie theory (GMT) is performed[38]. The incident and scattered fields are expressed as a sum of vector spherical harmonics (VSH). The scattered fields from particles are calculated by the method of order-of-scattering[39]. The local field at any point is the sum of the incident field and coupling fields scattered from all of the particles (see Methods). We first consider a silver nanoparticle dimer ($R_1 = R_2 = 40$ nm, with the gap distance $d = 1$ nm, Fig. 1a) excited at $\lambda = 532$ nm with linear polarization. The highest near-field enhancement is obtained when the excitation is polarized parallel to the dimer axis (y-axis) which induces the coupled dipole in the dimer. For the perpendicular polarized excitation, there is nearly no field enhancement for this uncoupled dimer. Generally, the relation between the near field in the dimer gap and incident field can be expressed as:

$$E_N = \begin{pmatrix} E_N^{//} \\ E_N^{\perp} \end{pmatrix} = \mathbf{G}_{\text{dimer}} \begin{pmatrix} E_i^{//} \\ E_i^{\perp} \end{pmatrix} \quad (1)$$

where $E_N{}^{\parallel}$ and $E_N{}^{\perp}$ are the near field components parallel and perpendicular to the dimer axis, respectively, and $E_i{}^{\parallel}$and $E_i{}^{\perp}$ are the corresponding components of the incident field. The enhancement tensor G_{dimer} can be written as:

$$\mathbf{G}_{\text{dimer}} = \begin{pmatrix} g_{11} & g_{12} \\ g_{21} & g_{22} \end{pmatrix} \quad (2)$$

Then, we have to analyze each element in this tensor. As shown in Fig. 1b, the field in the gap is highly dependent on the incident polarization, hence, we have $g_{11} \neq 0$ and $g_{12} = 0$ in this dimer case. Furthermore, at the surface of the metal, the enhanced near field in the junction is almost perpendicular to the surface irrespective of the incident polarization (white arrows in Fig. 1b). Then, both g_{21} and g_{22} are set to be zero. Hence, only the factor $g_{11} = |g_{11}|e^{i\Delta_1}$ is non-zero, where Δ_1 is the phase difference between the near field $E_N{}^{//}$ and incident field $E_i{}^{//}$, induced by the light scattering. The near-field enhancement $M_{\text{dimer}} = |E_N|^2/|E_i|^2 = |g_{11}|^2$.

When the incident light is circularly polarized, the near field in the dimer gap can be obtained by introducing the expression of the incident CPL into the formula (1),

$$E_N = \begin{pmatrix} E_N^{//} \\ E_N^{\perp} \end{pmatrix} = \begin{pmatrix} g_{11} & 0 \\ 0 & 0 \end{pmatrix} \begin{pmatrix} E_0 \\ E_0 e^{\pm i\frac{\pi}{2}} \end{pmatrix} \quad (3)$$

where "−" and "+" correspond to LCP and RCP incidences, respectively. Then we have the magnitude of the near field $|E_N| = |g_{11}|\,E_0$, which is irrelevant to the optical rotation.

The case will be quite different if we introduce another particle into the dimer system. As shown in Fig. 1c, the right-angle trimer is formed by positioning a particle ($R = 40$ nm) on the right side of the 2nd one with the distance $d = 1$ nm. Here we still consider the local field in the gap between the 1st and 2nd particles. As shown in Fig. 1d, the near-field enhancement for the perpendicular (x-axis) polarized

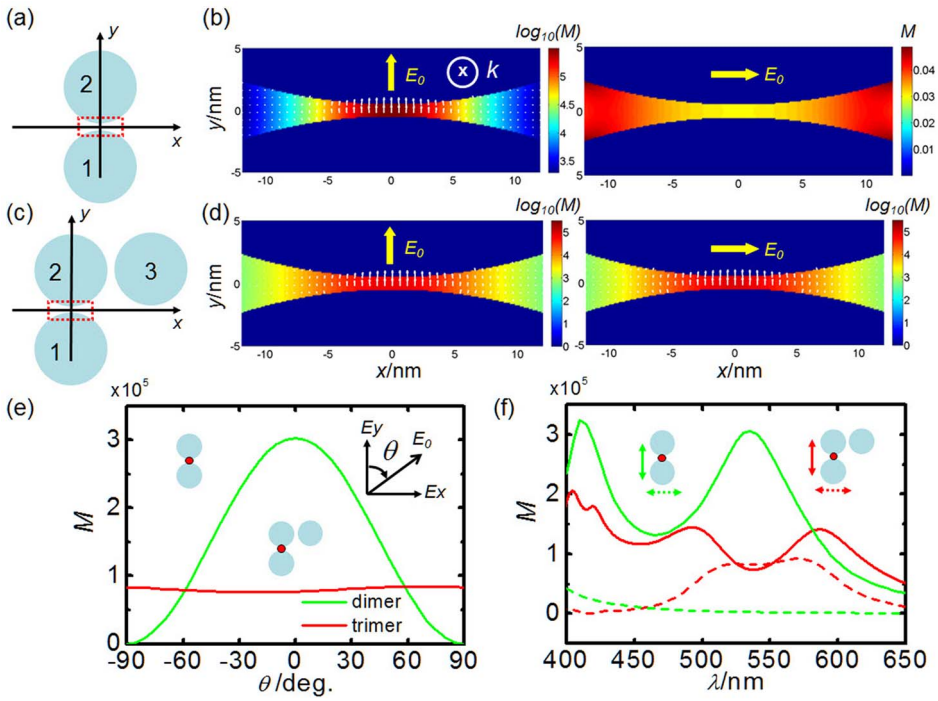

Figure 1 | Near-field enhancements in silver nanoparticle aggregates. Schematic diagrams of the dimer (a) and the right-angle trimer (c). The radius of particles are all 40 nm with the interparticle distance $d = 1$ nm. (b) Electric field intensity distributions around the interparticle junction of a dimer under parallel and perpendicular polarized excitations at $\lambda = 532$ nm. White arrow shows the direction of electric field. (d) Electric field intensity distributions around the 1st–2nd interparticle junction in the trimer with the same excitations as Fig. 1b. (e) Local field intensity at the hotspot in the interparticle junction (denoted by red dot in the inset) of the dimer (green curve) and trimer (red curve) as the function of the angle of the incident polarization, respectively. (f) Local field intensity in the dimer (green curves) and trimer (red curves) as a function of wavelength for parallel (solid curves) and perpendicular (dash curves) polarization, respectively.

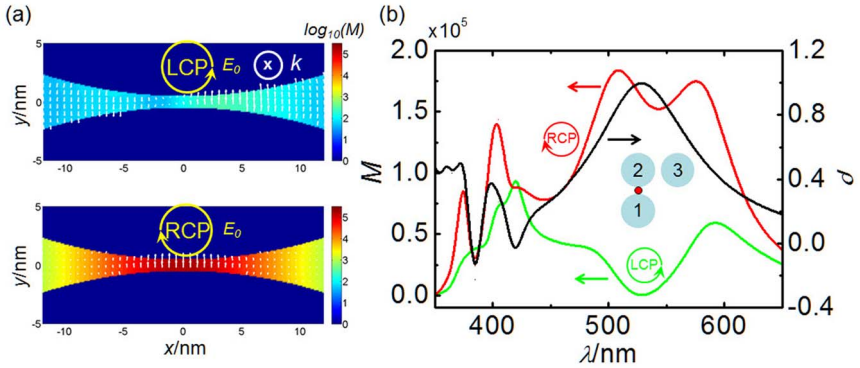

Figure 2 | Local CD response of the right-angle trimer. (a) Electric field intensity distributions around the interparticle junction in the right-angle trimer excited by LCP and RCP at 532 nm, respectively. (b) Local field intensity and local CD response ρ (black curve, to the right axis) at the hotspot in the interparticle junction as a function of the incident wavelength. The green and red curves are for LCP and RCP excitations, respectively. The CD response reaches its maximum value of 0.998 at 532 nm.

excitation is comparable with the parallel (y-axis) polarized case at λ = 532 nm. The near-field enhancements for the two orthogonal polarizations as a function of polarization and wavelength are shown in Fig. 1e and 1f, respectively. Obviously, due to the strong coupling of the 3rd particle with the dimer, the local field in the gap is insensitive to the incident polarization, especially in the wavelength range of 500 ~ 600 nm.

For the CPL excitation, the relation between the scattered and incident field can still be depicted by formula (1) with a response tensor G_{trimer} for the trimer. Just as we did in the dimer case, it is still necessary to know the elements in G_{trimer}. First, as the electromagnetic boundary relation still holds for trimer case, the polarization of near field in the gap is perpendicular to the metal surface (white arrows in Fig. 1d). Hence, we still have $g_{21} = g_{22} = 0$ for tensor G_{trimer}. Second, different from the dimer case, the perpendicular $E_i^{\perp}$ could also result in significant enhancement $E_N^{//}$, therefore both g_{11} and g_{12} are generally nonzero. So the near field for CPL excitations can be written as:

$$E_N = \begin{pmatrix} E_N^{//} \\ E_N^{\perp} \end{pmatrix} = \begin{pmatrix} g_{11} & g_{12} \\ 0 & 0 \end{pmatrix} \begin{pmatrix} E_0 \\ E_0 e^{\pm i\frac{\pi}{2}} \end{pmatrix} \quad (4)$$

where $g_{11} = |g_{11}|e^{i\Delta 1}$, $g_{12} = |g_{12}|e^{i\Delta 2}$, and Δ_2 is the phase difference between the near field $E_N^{\perp}$ and incident field $E_i^{\perp}$. After simple derivations, the near-field enhancement for the CPL incidence can be obtained:

$$M_{CPL} = \frac{|E_N^{//}|^2 + |E_N^{\perp}|^2}{2E_0^2} = \frac{1}{2}(|g_{11}^2| + |g_{12}^2|) + |g_{11}g_{12}|\cos[\Delta_1 - (\Delta_2 \pm \frac{\pi}{2})] \quad (5)$$

Obviously, M_{CPL} depends highly on the field enhancement factors $|g_{11}|$ and $|g_{12}|$, and especially the phase difference between Δ_1 and Δ_2. For example, at λ = 532 nm, $|g_{11}|^2 \approx |g_{12}|^2 = 0.8*10^5$, and $\Delta_1 - \Delta_2 \approx \pi/2$. The field enhancement at the gap for LCP and RCP excitation will be $M_{LCP} = 2.6*10^2$ and $M_{RCP} = 1.6*10^5$, respectively. The enhancement in the gap excited by the RCP light is much larger than the LCP case as shown in Fig. 2a, that is, the local CD. Actually, the local CD is the consequence of the near-field destructive/constructive interferences determined by the $\Delta_1 - \Delta_2$ when the factor $g_{11}*g_{12}$ are nonzero. Similar near-field interference mechanism had been used for controlling the surface plasmon polaritons in plasmonic waveguides[40,41].

According to the definition of CD signals for far-field transmission or reflection[22], we introduce a ratio ρ to evaluate the difference of near-field enhancement for incident LCP and RCP, which is defined as

$$\rho = (M_{RCP} - M_{LCP})/(M_{RCP} + M_{LCP}) \quad (6)$$

A giant local CD response ρ = 0.998 is obtained for the right-angle trimer at 532 nm. For other wavelengths, the partial interference results in the local CD spectrum shown by the black curve in Fig. 2b.

If a chiral molecule is situated in a symmetric dimer, the interaction between the molecule and nanoparticles would result in a far-field plasmonic CD[29–31], although the hotspot in dimer gap does not have near-field CD response as discussed above. For the asymmetric timer case, the near-field intensity in the gap could have 1000 times difference depending on the handedness of light. This will add to the complexity of molecule-induced plasmonic chirality. It can be expected that the far-field CD signal, especially the term originated from the exciton-plasmon interaction, could be enhanced or weakened, determined by the combination of the corresponding positive or negative near-field CD and the optical rotatory dispersion of the molecule at surface plasmon resonance wavelength.

Discussion

The local CD is highly dependent on the geometry of the nanoantenna. Fig. 3a shows how the near-field enhancement M and CD response ρ change as the rotation of the 3rd particle around the dimer. When θ = 0°, the linear trimer corresponds to the point group $D_{\infty h}$[42,43]. The perpendicular (x-axis) polarized incidence will excite weak coupled π_u mode. Hence, similar to the dimer, the enhancement factor $g_{12} \approx 0$, and $M_{LCP} = M_{RCP}$, *i.e.*, ρ = 0. When the 3rd particle is rotated around the dimer (θ = 0° ~ 90°), a C_{2v} trimer is formed. In this configuration, both A_1 and B_2 plasmon modes[42] can be excited and result in considerable field enhancement in the dimer gap irrespective to the incident polarization, *i.e.*, both g_{11} and g_{12} are nonzero. Consequently, the local CD response ρ grows with the increase of θ and reaches its maximum around 90°. After passing 90°, the 3rd particle gets closer to the 1st one and finally forms an equilateral trimer (D_{3h} group) at θ = 120°. Both degenerate E' modes in the D_{3h} trimer can be excited by two orthogonal polarizations[43]. When the incident polarization is parallel to the 1st–2nd dimer axis, three particles coupled each other strongly and result in the near-field enhancement in the particle gaps, i.e. a large factor g_{11}. While for the perpendicular polarized incidence, the E' mode is contributed by the dipolar coupling of 3rd with 1st and 2nd particles, while the interaction between 1st and 2nd particles is rather weak. Hence, there is almost no near-field enhancement in the 1st–2nd dimer gap, i.e., $|g_{12}| \ll |g_{11}|$. Then, local CD response ρ drops rapidly to zero again when θ = 120°.

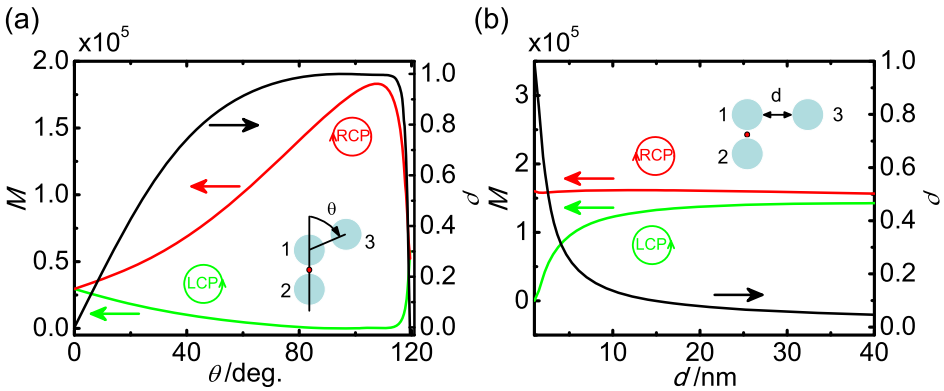

Figure 3 | Local CD response as a function of the geometry. (a) Local field intensity and CD response at the hotspot as a function of the rotation of the 3rd particle around the 2nd particle. (b) Local field intensity and CD response at the hotspot as a function of the distance d between the 3rd and 2nd particle. The green and red curves are for LCP and RCP excitations, respectively. The CD response ρ is shown by the black curve to the right axis. The excitation wavelength is 532 nm.

Apart from the structural asymmetry, ρ is also related to the magnitude of the coupling between 2nd and 3rd particles. As shown in Fig. 3b, when d is only several nanometers, both g_{11} and g_{12} are nonzero. According to the formula (5), ρ (black curve) is close to one, indicating a strong local CD response. The near-field enhancement for RCP excitation is much larger than the LCP case (green and red curves for LCP and RCP, respectively). As d increases, the 2nd–3rd interparticle coupling becomes weaker, which causes g_{12} dropping rapidly to zero. Correspondingly, ρ turns to be zero just as the dimer case.

Actually, the local CD response widely exists in asymmetric nanoparticle antennas. In Fig. 4a, we consider a non-identical trimer with the radii 30 nm, 40 nm, and 50 nm for the 1st to 3rd particles, respectively, and a fixed surface-to-surface distance d = 1 nm. The electric field enhancement at the hotspot for LCP and RCP excitations are shown by green and red curves, respectively. Due to the asymmetric coupling between particles, the wavelength dependences of the near-field enhancement g_{11} and g_{12} become quite complex. Hence, the difference in the spectrum of the near-field enhancement for LCP and RCP will result in the negative CD response $\rho = -0.89$ at 535 nm, and positive ρ = 0.74 at 605 nm (black curve). At λ = 535 nm, the near field for LCP excitation will be much larger than the RCP case as shown in the Fig. 4b.

As discussed above, the geometry and size determine the plasmonic modes excited in the nanoantenna, and consequently the local CD. Another important parameter influencing the surface plasmon coupling is the environment. Fig. 5 shows the spectrum of ρ for the right-angle trimer in air, water, and oil, with the refractive indexes n_s = 1, 1.33, and 1.5, respectively. The peak of wavelength-dependent ρ has an obvious red-shift with the increasing of n_s. Similar to the resonance shift in surface plasmon resonance sensors, the CD response in the gap in asymmetric structures is quite sensitive to the environment. The sensitivity factor, i.e., the shift in peak position per unit change in the refractive index of the surrounding medium, is 450 nm per refractive index unit, which is generally larger than usual sensitivity factor of localized surface plasmon peak[44].

In conclusion, we have investigated the near-field response in silver nanoparticle aggregates under the excitation of circular polarized light. We found that, the near-field enhancement of the hotspot in a right-angle trimer is highly dependent on the polarization rotation, that is, local CD originated from the near-field interference in the strong coupled particle system. The local CD can be evaluated by the parameter ρ. It is obtained a nearly unity ρ in the right-angle trimer excited at λ = 532 nm, where the near-field excited by RCP is much larger than the LCP case. This phenomenon widely exists in non-identical trimers, and can be tuned by the rotation of the 3rd particle and the interparticle distance. Furthermore, we found the CD response is quite sensitive to the environment and could be detected by the Raman signals of molecules, or fluorescence of quantum dots in one of the particle gaps. The manipulation of optical response through polarization and geometrical parameters opens possibilities for a wide range of applications, such as SERS[45–47] or ROA substrates[22,48], polarization sensitive devices[8], sensors[36] and bioapplications[18], *etc.*

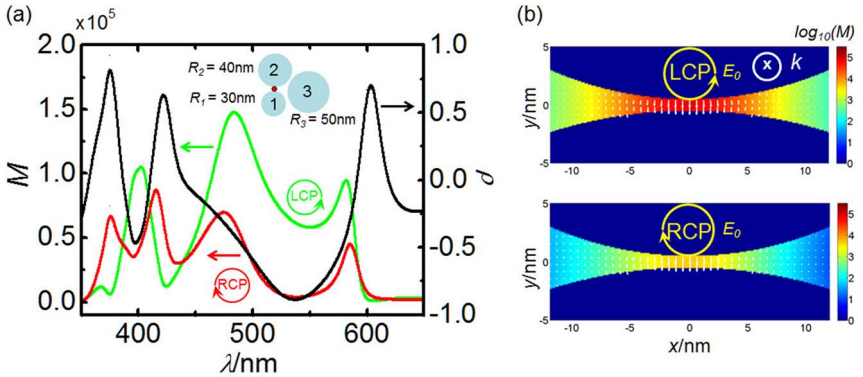

Figure 4 | Local CD response of a non-identical trimer. (a) Local field intensity and CD response at the hotspot as a function of the incident wavelength. The green and red curves are for the LCP and RCP excitations, respectively. The CD response ρ is shown by the black curve to the right axis. (b) Electric field intensity distributions around the interparticle junction for the incident LCP and RCP, respectively. The wavelength of the excitation is 535 nm.

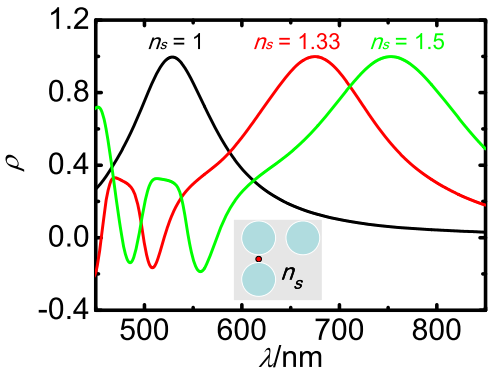

Figure 5 | Local CD response of the right-angle trimer in different dielectric environment. Black, red and green curves are the trimer in air, water, and oil, with the refractive index n_s = 1, 1.33, and 1.5, respectively.

Methods

Based on the generalized Mie theory[39], the incident and scattered electromagnetic fields are expanded into vector spherical harmonics (VSH). The expansion coefficients for incident field are well known as Mie coefficients. The scattered electric fields for N-spheres system are:

$$E_s = \sum_{l=1}^{\oplus N} E_s^l = \sum_{l=1}^{\oplus N} {}^{N}T_l \cdot {}^{l}W^{E} \tag{7}$$

where ${}^{l}W^{E}$ is the matrix of VSH, ${}^{N}T_n$ is the scattering matrix for the N-spheres system:

$$[{}^{N}T_1, {}^{N}T_2, {}^{N}T_3 \cdots {}^{N}T_N] = [G_1, G_2, G_3 \cdots G_N]\Psi^{(N)} \tag{8}$$

G_N is the incident coefficient for N^{th} sphere, $\psi^{(N)}$ is called response matrix of the system (for details see Ref.39). The scattered electric field under circularly polarized excitation is then:

$$E_s^{LCP} = E_s^{//} + E_s^{\perp} e^{+i\pi/2} \text{ and } E_s^{RCP} = E_s^{//} + E_s^{\perp} e^{-i\pi/2} \tag{9}$$

where E_s^{LCP}, E_s^{RCP}, $E_s^{//}$ and $E_s^{\perp}$ are the scattered electric fields under LCP, RCP, parallel, and perpendicular polarized excitations, respectively. Dielectric data of silver come from the work of Johnson and Christy in Ref.49.

1. Berova, N., Nakanishi, K. & Woody, R. W. *Circular Dichroism: Principles and Applications,* 2nd ed. (Wiley-VCH, New York, 2000).
2. Avitabile, C., D'Andrea, L. D. & Romanelli, A. Circular Dichroism studies on the interactions of antimicrobial peptides with bacterial cells. *Sci. Rep.* **4**, 4293 (2014).
3. Chen, W., Abeysinghe, D. C., Nelson, R. L. & Zhan, Q. Experimental confirmation of miniature spiral plasmonic lens as a circular polarization analyzer. *Nano Lett.* **10**, 2075–2079 (2010).
4. Plum, E. *et al.* Metamaterial with negative index due to chirality. *Phys. Rev. B* **79**, 035407 (2009).
5. Hendry, E. *et al.* Ultrasensitive detection and characterization of biomolecules using superchiral fields. *Nat. Nanotechnol.* **5**, 783–787 (2010).
6. Kim, T. -T. *et al.* Optical Activity Enhanced by Strong Inter-molecular Coupling in Planar Chiral Metamaterials. *Sci. Rep.* **4**, 5864 (2014).
7. Ma, W. *et al.* Chiral plasmonics of self-assembled nanorod dimers. *Sci. Rep.* **3**, 1934 (2013).
8. Gansel, J. K. *et al.* Gold Helix Photonic Metamaterial as Broadband Circular Polarizer. *Science* **325**, 1513–1515 (2009).
9. Kuzyk, A. *et al.* DNA-based self-assembly of chiral plasmonic nanostructures with tailored optical response. *Nature* **483**, 311–314 (2012).
10. Fan, J. A. *et al.* Self-assembled plasmonic nanoparticle clusters. *Science* **328**, 1135–1138 (2010).
11. Urban, A. S. *et al.* Three-dimensional plasmonic nanoclusters. *Nano Lett.* **13**, 4399–4403 (2013).
12. Mastroianni, A. J., Claridge, S. A. & Alivisatos, A. P. Pyramidal and chiral groupings of gold nanocrystals assembled using DNA scaffolds. *J. Am. Chem. Soc.* **131**, 8455–8459 (2009).
13. Chang, Y. C. *et al.* High-throughput nanofabrication of infra-red and chiral metamaterials using nanospherical-lens lithography. *Sci. Rep.* **3**, 3339 (2013).
14. Ben-Moshe, A., Maoz, B. M., Govorov, A. O. & Markovich, G. Chirality and chiroptical effects in inorganic nanocrystal systems with plasmon and exciton resonances. *Chem. Soc. Rev.* **42**, 7028–7041 (2013).
15. Gautier, C. & Bürgi, T. Chiral gold nanoparticles. *Chemphyschem.* **10**, 483–492 (2009).
16. Schäferling, M., Dregely, D., Hentschel, M. & Giessen, H. Tailoring Enhanced Optical Chirality: Design Principles for Chiral Plasmonic Nanostructures. *Phys. Rev. X* **2**, 031010 (2012).
17. Guerrero-Martínez, A., Alonso-Gómez, J. L., Auguié, B., Cid, M. M. & Liz-Marzán, L. M. From individual to collective chirality in metal nanoparticles. *Nano Today* **6**, 381–400 (2011).
18. Xia, Y., Zhou, Y. & Tang, Z. Chiral inorganic nanoparticles: origin, optical properties and bioapplications. *Nanoscale* **3**, 1374–1382 (2011).
19. Abdali, S. & Blanch, E. W. Surface enhanced Raman optical activity (SEROA). *Chem. Soc. Rev.* **37**, 980–992 (2008).
20. Seney, C. S., Gutzman, B. M. & Goddard, R. H. Correlation of Size and Surface-Enhanced Raman Scattering Activity of Optical and Spectroscopic Properties for Silver Nanoparticles. *J. Phys. Chem. C* **113**, 74–80 (2008).
21. Shegai, T. *et al.* Managing light polarization via plasmon–molecule interactions within an asymmetric metal nanoparticle trimer. *Proc. Natl. Acad. Sci. USA* **105**, 16448–16453 (2008).
22. Chuntonov, L. & Haran, G. Maximal Raman optical activity in hybrid single molecule-plasmonic nanostructures with multiple dipolar resonances. *Nano Lett.* **13**, 1285–1290 (2013).
23. Acevedo, R., Lombardini, R., Halas, N. J. & Johnson, B. R. Plasmonic Enhancement of Raman Optical Activity in Molecules near Metal Nanoshells. *J. Phys. Chem. A* **113**, 13173–13183 (2009).
24. Li, Z., Shegai, T., Haran, G. & Xu, H. Multiple-Particle Nanoantennas for Enormous Enhancement and Polarization Control of Light Emission. *ACS Nano* **3**, 637–642 (2009).
25. Barron, L. D., Zhu, F., Hecht, L., Tranter, G. E. & Isaacs, N. W. Raman optical activity: An incisive probe of molecular chirality and biomolecular structure. *J. Mol. Struct.* **834–836**, 7–16 (2007).
26. Sun, M. T. *et al.* Remotely excited Raman optical activity using chiral plasmon propagation in Ag nanowires. *Light-Sci. Appl.* **2**, e112 (2013).
27. Liu, Y., Wang, R. & Zhang, X. Giant circular dichroism enhancement and chiroptical illusion in hybrid molecule-plasmonic nanostructures. *Opt. Exp.* **22**, 4357–4370 (2014).
28. Drachev, V. P. *et al.* Large local optical activity in fractal aggregates of nanoparticles. *J. Opt. Soc. Am. B* **18**, 1896–1903 (2001).
29. Zhang, H. & Govorov, A. O. Giant circular dichroism of a molecule in a region of strong plasmon resonances between two neighboring gold nanocrystals. *Phys. Rev. B* **87**, 075410 (2013).
30. Wang, R. -Y. *et al.* Experimental Observation of Giant Chiroptical Amplification of Small Chiral Molecules by Gold Nanosphere Clusters. *J. Phys. Chem. C* **118**, 9690–9695 (2014).
31. Wu, T., Ren, J., Wang, R. & Zhang, X. Competition of Chiroptical Effect Caused by Nanostructure and Chiral Molecules. *J. Phys. Chem. C* **118**, 20529–20537 (2014).
32. Halas, N. J., Lal, S., Chang, W. -S., Link, S. & Nordlander, P. Plasmons in Strongly Coupled Metallic Nanostructures. *Chem. Rev.* **111**, 3913–3961 (2011).
33. Schlather, A. E., Large, N., Urban, A. S., Nordlander, P. & Halas, N. J. Near-field mediated plexcitonic coupling and giant Rabi splitting in individual metallic dimers. *Nano Lett.* **13**, 3281–3286 (2013).
34. Tanaka, Y., Sanada, A. & Sasaki, K. Nanoscale interference patterns of gap-mode multipolar plasmonic fields. *Sci. Rep.* **2**, 764 (2012).
35. Shegai, T. *et al.* A bimetallic nanoantenna for directional colour routing. *Nat. Commun.* **2**, 481 (2011).
36. Ma, W. *et al.* Attomolar DNA detection with chiral nanorod assemblies. *Nat. Commun.* **4**, 2689 (2013).
37. Swiontek, S. E., Pulsifer, D. P. & Lakhtakia, A. Optical sensing of analytes in aqueous solutions with a multiple surface-plasmon-polariton-wave platform. *Sci. Rep.* **3**, 1409 (2013).
38. Xu, H. X. A new method by extending Mie theory to calculate local field in outside/inside of aggregates of arbitrary spheres. *Phys. Lett. A* **312**, 411–419 (2003).
39. Li, Z. & Xu, H. Electromagnetic energy flow near metal nanoparticles - II: Algorithms for the calculation of the light scattering of multi-spheres and photon energy transport via linear chains of Ag nanoparticles. *J. Quant. Spectrosc. Radiat. Transfer* **103**, 394–401 (2007).
40. Lin, J. *et al.* Polarization-controlled tunable directional coupling of surface plasmon polaritons. *Science* **340**, 331–334 (2013).
41. Rodríguez-Fortuño, F. J. *et al.* Near-field interference for the unidirectional excitation of electromagnetic guided modes. *Science* **340**, 328–330 (2013).
42. Chuntonov, L. & Haran, G. Trimeric plasmonic molecules: the role of symmetry. *Nano Lett.* **11**, 2440–2445 (2011).
43. Chuntonov, L. & Haran, G. Effect of Symmetry Breaking on the Mode Structure of Trimeric Plasmonic Molecules. *J. Phys. Chem. C* **115**, 19488–19495 (2011).
44. Xia, Y. & Halas, N. J. Shape-Controlled Synthesis and Surface Plasmonic Properties of Metallic Nanostructures. *MRS Bull.* **30**, 338–348 (2005).
45. Xu, H., Bjerneld, E. J., Käll, M. & Börjesson, L. Spectroscopy of Single Hemoglobin Molecules by Surface Enhanced Raman Scattering. *Phys. Rev. Lett.* **83**, 4357–4360 (1999).
46. Mao, L., Li, Z., Wu, B. & Xu, H. Effects of quantum tunneling in metal nanogap on surface-enhanced Raman scattering. *Appl. Phys. Lett.* **94**, 243102 (2009).
47. Sun, M. *et al.* Direct visual evidence for the chemical mechanism of surface-enhanced resonance Raman scattering via charge transfer: (II) Binding-site and quantum-size effects. *J. Raman Spectrosc.* **40**, 1172–1177 (2009).

48. Chuntonov, L. & Haran, G. Optical activity in single-molecule surface-enhanced Raman scattering: Role of symmetry. *MRS Bull.* **38**, 642–647 (2013).
49. Johnson, P. B. & Christy, R. W. Optical Constants of the Noble Metals. *Phys. Rev. B* **6**, 4370–4379 (1972).

Acknowledgments

This work was supported by National 973 Program of China (Grant No. 2012CB315701), National Natural Science Foundation of China (Grant No. 11274004, 61222505, 21473115), Hunan Provincial Natural Science Foundation of China (Grant No. 12JJ7005, 13JJ1012), NCET (Grant No. NCET-13-0915), and Scientific Research Base Development Program of the Beijing Municipal Commission of Education.

Author contributions

H.W. and Z.L. carried out the GMT simulations, and performed derivation of formulas. Z.L., H.Z., P.W. and S.W. interpreted and analyzed the data, and co-wrote the paper. Z.L., H.Z. and S.W. supervised the project. All authors discussed the results and commented on the manuscript.

Additional information

Competing financial interests: The authors declare no competing financial interests.

How to cite this article: Wang, H., Li, Z., Zhang, H., Wang, P. & Wen, S. Giant local circular dichroism within an asymmetric plasmonic nanoparticle trimer. *Sci. Rep.* **5**, 8207; DOI:10.1038/srep08207 (2015).